System tools applied to micro-cantilever based devices

A. Sebastian[1], S. Salapaka[2], and M. V. Salapaka[1]

[1] Iowa State University, Ames IA 50014, USA
[2] Laboratory for Information and Decision Systems, MIT, MA 02139, USA

Abstract. Micro-cantilever based devices can be used to investigate and manipulate matter at atomic scales. Taking the case study of atomic force microscope (AFM) we demonstrate the power of system tools in the analysis of micro-cantilever based devices. They capture important characteristics and predict inherent limitations in the operation of these devices. Such a systems approach is shown to complement the physical studies performed on these devices. Tractable models are developed for the AFM operating in tapping-mode. For the interrogation of samples, it is also imperative that sample positioning should be done with high precision and at high speeds. This broadband nanopositioning problem is shown to fit into the modern robust control framework. This is illustrated by the design, identification and control of such a positioning device.

1 Introduction

Desirable properties of manufactured products arise from the manner in which atoms are arranged in its material. Until recently, ways of manipulating and interrogating matter were limited to aggregate methods where the control and investigation of matter was achieved at scales much larger than atomic scales. Recent demonstrations made possible by micro-cantilever based devices provide ample evidence indicating the feasibility of rational *control, manipulation* and *interrogation* of matter at the atomic scale.

Micro-cantilevers have been utilized in biological sciences in a variety of applications like sensing sequence-specific DNA [9], studying cell-cell interactions [4] and antigen/antibody interactions [7]. Another intriguing application is in the detection of single electron spin ([13,20–22]). Such research has significant ramifications for quantum computing technology and to the physics at atomic scales. For more description of the impact of micro-cantilever based devices see [24].

In spite of the vast underlying promise, considerable challenges need to be overcome to fully harness the potential of this technology. A key element of the micro-cantilever based technique is the manner in which the cantilever interacts with the matter it is investigating or manipulating. Although micro-cantilever based devices have been utilized ubiquitously in various applications, the dynamics of the cantilever-sample interaction is significantly complex and considerable research effort is being placed at deciphering this interaction. Most of the research effort

L. Giarré, B. Bamieh (Eds.): Multidiciplinary Research in Control, LNCIS 289, pp. 83–99, 2003

is towards developing sophisticated and often involved physical models of the tip-sample interaction ([1], [6]). This has helped provide insights into the various physical sources of the tip-sample interaction force. However these approaches do not lend themselves towards isolating the principle characteristics and limitations of micro-cantilever based devices. A systems based approach significantly complements the physical studies performed on the tip-sample interaction, provides new ways of interpreting data, new ways of imaging and indicates the fundamental limitations of micro-cantilever based devices. Such an approach has been missing from the literature until the work of the authors. We highlight these studies in this article.

Another pivotal requirement for harnessing the vast potential of micro-cantilever based technology is ultra-fast positioning. To achieve high throughput, fast positioning is imperative. It is also becoming increasingly evident that for many nanotechnological studies, *high bandwidth is a necessity*. For example, in the field of cell biology, attractive proposals on using nanotechnology have been presented where nano-probes track events in the cell. These events often have time-scales in the micro-second or nano-second regimes. Current nanopositioning technology does not meet the needed high precision and bandwidth requirements. The modern robust control paradigm offers a powerful tool to address the challenges of broadband nanopositioning. We will highlight how such an approach has yielded considerable dividends in this case. The Atomic Force Microscope (AFM) is one of the primary micro-cantilever based devices. In the next section we give a brief overview of the AFM.

2 Atomic Force Microscope: operating principles and features

The schematic of a typical AFM is shown in Figure 1. It consists of a micro-cantilever, a sample positioning system, a detection system and a control system. A typical cantilever is $100-200\ \mu m$ long, $5-10\ \mu m$ wide and has a tip of diameter $\approx 5\ nm$. Most of the cantilevers are micro-fabricated from silicon oxide, silicon nitride or pure silicon using photolithographic techniques. The cantilever deflects under the influence of the sample and other forces. This deflection is registered by the laser incident on the cantilever tip which reflects into a split photodiode. This setup constitutes the detection system. The minimum detectable cantilever deflection is in the order of $0.01\ nm$. Using the measured deflection signal, the control system moves the sample appropriately to achieve necessary objectives. Sample positioning is usually provided by a piezoelectric based positioning stage.

Since its invention in 1986 a wide range of modes of operations have emerged. In contact mode or static mode operation, the cantilever deflection is primarily due to the tip-sample interaction. The deflection of the tip is used to interpret sample properties. In the tapping-mode or dynamic mode operation, the cantilever support is forced sinusoidally using a dither piezo. The changes in the oscillations introduced due to the sample are interpreted to obtain the sample properties [24].

Central to the operation described above is the micro-cantilever which largely determines the achievable sensitivity and resolution of the AFM. It is thus important to identify the cantilever parameters precisely. For many applications the micro-cantilever is well modeled as a flexible structure. The displacement of the cantilever at time t denoted by $p(t)$ is given by $p(t) = \sum_{k=1}^{\infty} \xi_k q_k(t)$ where ξ_k is the

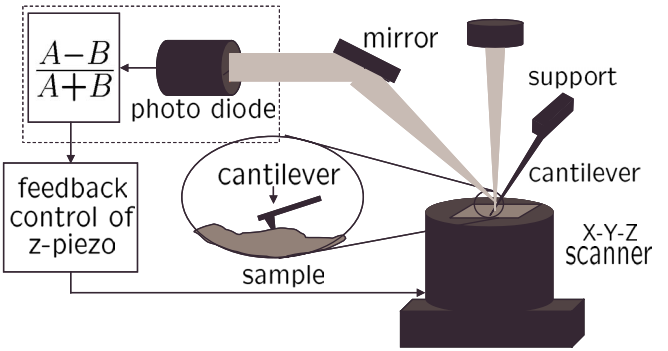

Fig. 1. A typical setup of an AFM. The chief components are the micro-cantilever, a sample positioning system, an optical detection system and a feedback controller.

mode shape evaluated where the laser is incident on the cantilever. Using only a finite set of the mode shapes ξ_k, one can show that the state space description of the dynamics is given by,

$$\begin{aligned} \dot{x} &= Ax + B_1\eta + BF \\ p(t) &= \sum_{k=1}^{N} \xi_k q_k(t) = Cx \end{aligned} \tag{1}$$

where $x := \left(q_1 \; q_2 \; .. \; q_N \; \dot{q_1} \; \dot{q_2} \; .. \; \dot{q_N} \right)^T$, η is the thermal noise forcing term. F describes all the external forces acting on the cantilever. A, B_1 and B are functions of the mass, damping and stiffness of the cantilever.

$p(t)$ is available as a measured signal using the detection scheme shown in Figure 1. Methods are available to obtain a precise description of the multi-mode model using the thermal noise response (see [14]). In typical applications a first-mode approximation is sufficient.

3 Systems approach to the analysis of AFM dynamics

The tapping-mode operation is the most common method of imaging primarily because it is less invasive on the sample and has higher signal to noise ratio. In this mode, due to the cantilever oscillation the tip moves over a long range of highly nonlinear tip-sample potential leading to complex behavior. The complexity of the dynamics can be assessed by the experimental and theoretical studies that confirm the existence of chaotic behavior (see [2], [3], [5] and [16]). However under normal operating conditions the cantilever is found to evolve into a stable periodic orbit with a period equal to the period of forcing. It is also experimentally observed that when the tip-sample separation is sufficiently large, the periodic orbit is near sinusoidal.

Much of the research on tapping-mode dynamics has revolved around solving nonlinear differential equations numerically (see [1]). As mentioned earlier even though they predict experimentally observed behavior, they fail to capture the limitations and important characteristics in the operation of tapping-mode AFM. Also the identification of model parameters is not straightforward due to their complexity. In this article we highlight a systems perspective of the tapping-mode

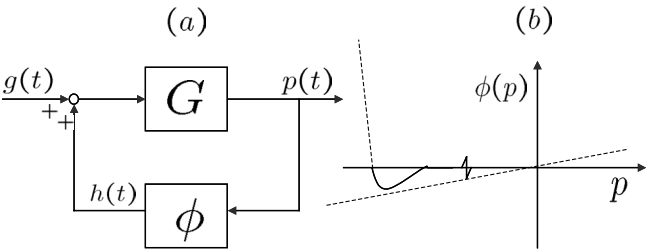

Fig. 2. (a) The feedback perspective of dynamic mode AFM dynamics. G corresponds to the linear cantilever model. ϕ is a nonlinear model for the tip-sample interaction. (b) A typical plot of tip-sample interaction, ϕ Vs. position, p.

dynamics. A detailed version of this development is provided in [18], [19] and a preprint. The cantilever can be imagined to be a system that takes in as inputs the dither signal, $g(t)$ and the tip-sample interaction force, $h(t)$. It produces the deflection signal, $p(t)$ as the output. (see Figure 2(a)). Let G denote such a block. The state space description of G is given by (1). By ignoring the noise forcing and recognizing $F = g(t) + h(t)$, from (1) we obtain,

$$\begin{aligned} \dot{x} &= Ax + B(h(t) + g(t)) \\ p &= Cx \end{aligned} \tag{2}$$

The tip-sample interaction forces now appear as a feedback block. In this perspective the instantaneous tip position is fed back to the system G through the function ϕ. In this way we view the tapping-mode dynamics as an inter-connection of two systems, the system G that models the cantilever and the block ϕ that models the sample.

3.1 Analysis of the periodic solutions

Given the complex dynamics of tapping-mode AFM, the questions on the existence and stability of periodic solutions are very relevant. As a first application of the systems viewpoint, the existence and stability of periodic solutions in tapping-mode AFM are explored.

Sector bounds on the attractive part of the tip-sample interaction ϕ (see Figure 2(b)) can be computed for typical tip-sample interactions. Coupled with such

a characterization, it is possible to describe ϕ in terms of integral quadratic constraints (IQC) which capture how the nonlinearity distributes the input signal's energy over various frequencies (see [10] for a comprehensive treatment of IQCs).

Definition 1. ϕ is said to satisfy the IQC defined by a multiplier $\Pi = \begin{pmatrix} \Pi_{11} & \Pi_{12} \\ \Pi_{21} & \Pi_{22} \end{pmatrix}$ if

$$\int_{-\infty}^{\infty} \begin{pmatrix} \hat{y}(j\omega) \\ \hat{\phi(y)}(j\omega) \end{pmatrix}^* \Pi(j\omega) \begin{pmatrix} \hat{y}(j\omega) \\ \hat{\phi(y)}(j\omega) \end{pmatrix} d\omega \geq 0 \tag{3}$$

for all $y \in L_2$. We denote this by $\phi \in IQC(\Pi)$.

In the above definition $\hat{y}$ corresponds to the Fourier transform of y.

As a first step towards establishing the existence and stability of periodic solutions we prove the global exponential stability of $x = 0$ for the dynamics described by equation (2) with $g(t) = 0$. A computationally attractive way of proving the global exponential stability is using the IQCs.

Assuming that $\Pi_{11} \geq 0$ and $\Pi_{22} \leq 0$, the global exponential stability can be concluded if $\phi \in IQC(\Pi)$ and $\exists\ \epsilon > 0$ such that,

$$\begin{pmatrix} (j\omega I - A)^{-1}B \\ I \end{pmatrix}^* \tilde{\Pi}(jw) \begin{pmatrix} (j\omega I - A)^{-1}B \\ I \end{pmatrix} \leq \ -\epsilon I \ \forall\ \omega \tag{4}$$

where $\tilde{\Pi} = \begin{pmatrix} C^T\Pi_{11}C & C^T\Pi_{12} \\ \Pi_{21}C & \Pi_{22} \end{pmatrix}$. From the global exponential stability the converse Lyapunov theorem can be invoked to obtain a Lyapunov function $W(x)$ which when evaluated along the trajectories of the forced system satisfies,

- $W(x) \to \infty$ as $|x| \to \infty$
- There exists $\xi > 0$ and a continuous function $a(x) > 0$ for $\|x\| \geq \xi$ such that for any solution $\|x(t)\| \geq \xi$, $\frac{d}{dt}(w(x(t)) \leq -a(x(t))$.

From the existence of the above $W(x)$, it can be shown that (2) has a solution $x_0(t)$ bounded for $-\infty < t < \infty$ ([25]). Let $x(t)$ be another solution of (2). Let $\tilde{x}(t) = x(t) - x_0(t)$. From (2) we obtain,

$$\dot{\tilde{x}} = A\tilde{x} + B\tilde{\phi}(t, \tilde{y}),\ \tilde{p} = C\tilde{x} \tag{5}$$

where $\tilde{\phi}(t, v) := \phi(v + p_0(t)) - \phi(p_0(t))$. The global exponential stability of (5) implies the stability of the solution $x_0(t)$ which can be established by searching for a Π such that $\tilde{\phi} \in IQC(\Pi)$ and (4) is satisfied. Using the fact that the forcing is periodic and from the uniqueness of the solution we can conclude the periodicity of $x_0(t)$.

As mentioned earlier the experimentally observed periodic orbit is nearly sinusoidal. It could be argued heuristically that the sharp bandpass characteristic of the cantilever subsystem leads to smaller higher harmonics and hence a near sinusoidal orbit. Using the IQCs, one can provide rigorous bounds on the higher harmonics. If these bounds are shown to be significantly smaller than the first harmonic, then it can be concluded that the periodic solution is almost sinusoidal. Compare this approach with Ref. [8] where the author evaluates the interaction forces only for the first harmonic which amounts to assuming sinusoidal nature of the periodic solution. The following theorem from Ref. [11] is used to obtain bounds on the higher harmonics.

Result 1. *In Figure 2 let* $g(t) = g_1 e^{j\omega_0 t} + g_{-1} e^{-j\omega_0 t}$, $p(t) = \sum p_k e^{jk\omega_0 t}$ *and* $h(t) = \sum h_k e^{jk\omega_0 t}$. *If*

1. ϕ *satisfies the IQC defined by* Π
2. $\begin{pmatrix} G(jk\omega_0) \\ 1 \end{pmatrix}^* \Pi(jk\omega_0) \begin{pmatrix} G(jk\omega_0) \\ 1 \end{pmatrix} \leq -\epsilon$ *for all* $|k| \neq 1$.

Then for $|k_0| \neq 1$, *the bound* $|p_{k_0}| < \beta |g_1|$ *holds for all* β *that together with some* $\tau > 0$ *satisfies the inequality*

$$0 > \begin{pmatrix} 0 & 0 & 0 \\ 0 & -\beta^2 & 0 \\ 0 & 0 & 1 \end{pmatrix} + \tau \begin{pmatrix} K_1 & L_1 & 0 \\ L_1^* & M_1 & 0 \\ 0 & 0 & K_{k_0} \end{pmatrix} \tag{6}$$

where

$$\begin{pmatrix} K_k & L_k \\ L_k^* & M_k \end{pmatrix} = \begin{pmatrix} 1 & 0 \\ G^{-1}(jk\omega_0) & -1 \end{pmatrix}^* \Pi(jk\omega_0) \begin{pmatrix} 1 & 0 \\ G^{-1}(jk\omega_0) & -1 \end{pmatrix}$$

For each higher harmonic of $p(t)$, we can solve the Linear Matrix Inequality (LMI) given by (6), and obtain β. An upper bound on the harmonic is obtained by multiplying β by the magnitude of forcing. Note that the bounds on the higher harmonics can also be used to assess the limitations on how well the tip-sample potential can be probed using the micro-cantilever. A more detailed exposition of the above approach is provided in Ref. [18] where the existence, stability and near sinusoidal nature of periodic solutions are explored under certain operating conditions. Also the existence and local orbital stability of periodic orbits are studied in Ref. [15] for a one-mode approximation of the cantilever.

3.2 Harmonic analysis based identification of tip-sample interaction

In certain cases, the existence and stability of periodic solutions can be proven in a rigorous manner ([18], [15]). In this section the assumption that tapping-mode dynamics permits the existence of a periodic solution with the same period as that of forcing is used to derive the harmonic balance equations. Let such a periodic solution be denoted by $p_0(t)$ and let it have a period of T. Assuming the nonlinear force on the cantilever due to the sample is time invariant it follows that $h(t)$ is also T periodic. Thus p_0, h and g admit expansions of the form $p_0(t) = \sum_{k=-\infty}^{\infty} p_k e^{jk\omega t}$, $h(t) = \sum_{k=-\infty}^{\infty} h_k e^{jk\omega t}$ and $g(t) = \sum_{k=-\infty}^{\infty} g_k e^{jk\omega t}$ where $\omega = 2\pi/T$. Since the cantilever model G is assumed to be linear time invariant the input and output harmonics of the system are related by, $G(jk\omega)(g_k + h_k) = p_k$, for all $k = 0, \pm 1, \pm 2, ...$

The steady state periodic orbit of the cantilever depends on the forcing frequency ω, the magnitude of forcing γ, and tip-sample separation l. h_k and p_k are functions of γ, ω and l. By varying one of these parameters we can evaluate h_k for different values of γ, ω or l. This in turn can be used to identify tip-sample interaction forces. One approach to identifying the tip-sample interaction is to assume a parametric model. Let $H(\theta)$ denote such a model where θ is a finite set of parameters. If H_k are the Fourier coefficients of $H(\theta)(p(t))$, then the estimation of the parameters reduce to solving the minimization problem,

$$\min_{\theta} \sum_{k=0}^{\infty} |H_k - h_k|^2. \tag{7}$$

3.3 Experimental results

An AFM was operated in the tapping-mode. A silicon cantilever of $225\,\mu m$ was used. The model parameters were evaluated by analyzing the response to thermal noise as mentioned earlier. The sample (silicon wafer) was sufficiently far from the cantilever initially. Once the oscillations reached the steady state the sample was moved towards the cantilever. At different values of tip-sample separation, the motion of the cantilever tip was recorded after the tip settles into a new periodic orbit.

A piecewise linear model was assumed for the tip-sample interaction as depicted in Figure 3. It is motivated by the long range attractive forces and short range repulsive forces typically observed. Using the tools described earlier, it is possible to estimate the model parameters from the experimental data (see [19]). The estimated parameters were used to simulate the AFM operating in tapping-mode. The corresponding results were compared with those obtained experimentally. As predicted by the analysis earlier, the higher harmonics were insignificant compared to the first harmonic. In Figures 4 and 5 the amplitude and phase of the first harmonic of the resulting oscillations at different points of separation are compared with that obtained experimentally. The plots show good agreement between the experiments and the simulations. It is to be noted that a simple tip-sample interaction model can predict the cantilever behavior. This can be explained from the observation that even if the tip-sample interaction has finer features, their effect get filtered out due

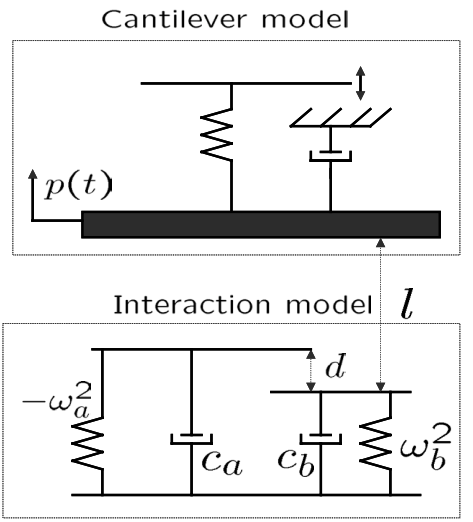

Fig. 3. A first-mode approximation of the cantilever model and a model for the tip-sample interaction. The negative spring models the attractive forces and the positive spring models the repulsive forces. The dampers account for the energy dissipation due to sample interaction.

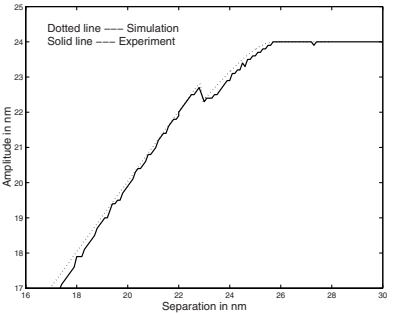

Fig. 4. Using the estimated parameter values the AFM operation is simulated and the results are compared with that observed experimentally. Here the amplitude is plotted against the tip-sample separation.

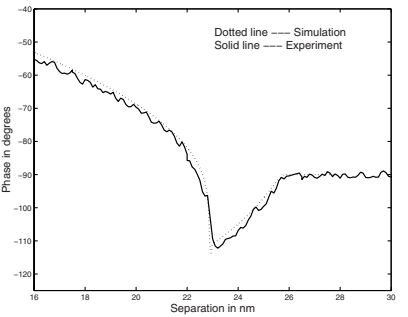

Fig. 5. This plot depicts the good match obtained in the phase values.

to the sharp band-pass characteristic of the cantilever. This imposes a limitation on the detection of interaction forces using tapping-mode AFM.

From the above analysis it is evident that the systems perspective provides unique insights which may not be obtained from a physical model. In the next section we deal with the nanopositioning aspect of micro-cantilever based devices.

4 Broadband nanopositioning

We have seen that nanopositioning systems form a very important part of micro-cantilever based devices. Most of these systems are piezoactuated. Piezoelectric materials achieve repeatable nanometer and sub nanometer resolutions at relatively high bandwidths. This is possible since they have no moving parts and thereby avoid undesirable effects such as backlash and stick-slip motions. Also, they can generate large forces (as high as few tens of kN), have very fast response times (acceleration rates of $10^4 g$ can be obtained), are not affected by magnetic fields,

and are operable at wide ranges of temperatures (they are functional even at near zero Kelvin temperatures). However, obtaining high positioning precision is significantly complicated or even unachievable due to nonlinear effects like hysteresis and creep. This is true especially when the piezoactuators are used in relatively long range positioning applications or for extended periods of time. Most of the commercially available devices circumvent these nonlinear effects at the cost of their performance by restricting the devices to low drive applications where the behavior is approximately linear and/or limiting their motions to specific trajectories for which nonlinear effects have been accounted for and appropriately compensated.

In this section, we present the design and modeling of a nanopositioning device that we developed in collaboration with Asylum Research[1]. This device is also piezoactuated and therefore inherits all the advantages and disadvantages mentioned earlier. A modern robust control approach is taken in the design of the controller. This section is a condensed form of Ref. [17].

4.1 Device Description

The device consists of four components: a base plate which seats the nanopositioning system and the sample holder, an AFM head that seats the sample-probing system a top plate that seats the AFM head and a control system.

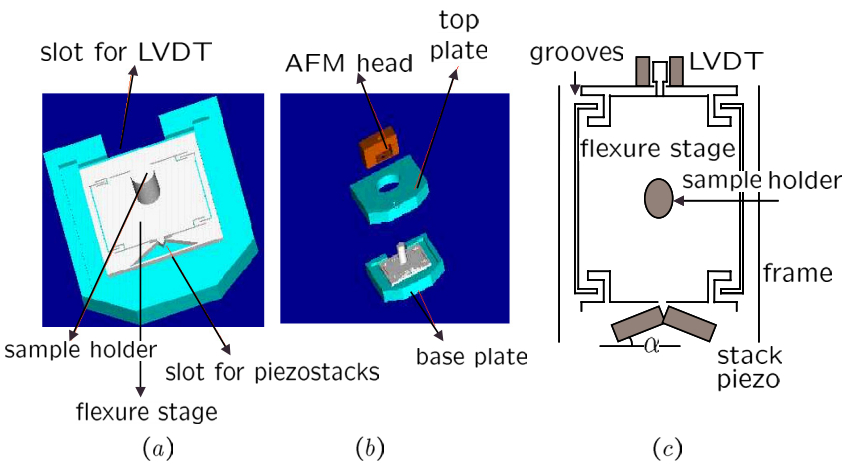

Fig. 6. (a) The base plate of the flexure stage. (b) The exploded view of the flexure and evaluation stages. (c) A schematic to show the serpentine design of the base plate.

The base plate consists of three main subcomponents: A flexure stage which has a small scan stage on which the sample is placed (see Figure 6). It is a 20 $cm \times$

[1] Santa Barbara, CA 93117

20 $cm \times 5$ cm steel plate with a cylindrical block in the center to hold the sample. This sample holder moves with respect to the periphery of the plate by virtue of the serpentine spring design.

A piezo-stack arrangement (with a voltage amplifier) forms the actuation system. It is seated in a slot in the base plate. The amplified voltage signal applied across the stack leads to its deformation, which in turn imparts motion to the flexure stage. This actuation system is relatively cheap and provides a good travel (of about 70 μm) but has poor hysteresis and creep properties compared to commercially available J-scanners that are predominantly used.

A Linear Variable Differential Transformer (LVDT) constitutes the detection system. It is seated in a slot in the base plate on the opposite side of the actuation system.

An AFM head (described in the previous section) consisting of a microcantilever and associated laser/optical arrangement forms the sample probing system. The top plate is of similar dimensions as a base plate and is there to provide support to the AFM head above the sample (see Figure 6(b)).

A block diagram of the nanopositioning system including the control system is shown in Figure 7. Here the transfer function $G(s)$ refers to an identified model of the system that comprises of the actuation, flexure and detection stages of the device. The reference signal x_r, the feedback law $K(s)$ and the prefilter $F(s)$ were implemented on a Texas Instruments TMS320C44 digital signal processor based development platform.

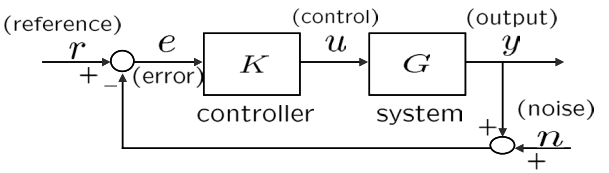

Fig. 7. A schematic block diagram of the closed loop system.

4.2 Identification and control design

The model $G(s)$ was obtained from the frequency response about the null position by giving a sine sweep of small amplitudes (less than 50 mV) up to a bandwidth 2 KHz . A fourth order non minimum phase transfer function: $G(s) = \frac{9.7\times10^4(s-(7.2\pm7.4i)\times10^3)}{(s+(1.9\pm4.5i)\times10^3)(s+(1.2\pm15.2i)\times10^2)}$ yielded a good fit to this response.

We obtained frequency responses at different operating points (other than the null position) and also studied how these responses changed by changing the amplitudes of the sine sweep signal. It was observed that there are considerable changes in the frequency responses with the set points and amplitudes of sine sweep signals. This emphasized the importance of designing feedback laws that are robust to model uncertainties. Another important aspect of this model is the presence of

the RHP zeroes. This can be explained as the actuation and detection systems are not collocated but instead are separated by a flexure stage. The inverse response behavior which is a characteristic of flexible structures and non minimum phase systems was observed in experiments which further corroborates the model. The RHP zeros rule out high gain proportional control laws and impose a fundamental limit on the achievable bandwidth of the closed loop system. In the presence of a complex pair of RHP zeros ($z_{1,2} = x \pm iy$), the "ideal" controller can achieve a sensitivity function of, $S = \frac{4xs}{(s+x+jy)(s+x-jy)}$ which leads to a limit on the achievable bandwidth [12,23] of $415Hz$ for our model.

Traditional controller design Before proceeding it is worthwhile to indicate the control tools presently employed by the AFM industry. The most widely used microscope (Multimode, Digital Instruments) do not have feedback loops for lateral positioning. Most other variants do not employ model based control designs. The most prominent technique is the PI technique where the PI gains are left to the user to set and is often a source of confusion. As PI is the most commonly used controller, we have analyzed the PI controller's performance. The optimized parameter values of $k_p = 0.01$ and $k_i = 75$ guarantees a gain margin of 1.57 and a phase margin of 89° while giving a *bandwidth of only about* $2.12Hz$.

$\mathcal{H}_\infty$ controller design While designing feedback controllers for nanopositioning systems, robustness and resolution assume great importance besides high bandwidth. Feedback controllers should be robust to nonlinear effects like hysteresis and creep. The nanopositioning devices currently in use have good noise characteristics that lead to high resolution. While trying to achieve good robustness and bandwidth it is imperative that the feedback controller does not deteriorate the resolution of the device. This tradeoff is very well captured by the sensitivity S and complementary sensitivity T transfer functions. Low complementary sensitivity gains imply lesser effect of noise (since $e = x_r - x = Tn$) and therefore higher resolution; similarly, low sensitivity gains imply better tracking of reference signals (since $e = Sx_r$) and therefore higher bandwidth. In this way the tradeoff between the shapes of the sensitivity and complementary sensitivity functions determines the tradeoff between the resolution and the bandwidth of the device. It becomes important to design control laws that appropriately shape these closed loop transfer functions. Thus the problem of designing controllers for nanopositioning devices fits well into the modern robust control framework. Also the positioning problem in X, Y and Z directions could be addressed in a MIMO framework.

In the $\mathcal{H}_\infty$ design, an optimization problem to obtain desirable shapes for the closed loop transfer functions is solved (see [23] for a good exposition to this design methodology).

The objectives were posed in an $\mathcal{H}_\infty$ design framework to obtain a controller K such that

$$\left\| \begin{bmatrix} W_1 S \\ W_2 T \\ W_3 K S \end{bmatrix} \right\|_\infty < \gamma$$

for some prespecified $\gamma > \gamma_{opt}$, the optimal value. The controller was designed (using the function, *hinfsyn* in Matlab) for $\gamma = 2.415$ and the weighting functions $W_i,\ i = 1, 2, 3$ were chosen as follows:

W_1 was chosen to be a first order transfer function, designed so that its inverse (an approximate upper bound on the sensitivity function) has a gain of 0.1% at low frequencies ($< 1\ Hz$) and a gain of $\approx 5\%$ around 200 Hz. This weighting function puts a lower bound on the bandwidth of the closed loop system and ensures good tracking at these frequencies. Similarly, the complementary sensitivity function, T was shaped by choosing the weighting function such that its reciprocal has low gains at high frequencies and vice versa. T was made to roll off at a frequency of 400 Hz. This diminishes the effect of noise on the error signal thus providing a handle on the resolution of the device. We also shaped the KS transfer function (by choosing $W_3 = 0.1$) so as to limit the control effort (since the control signal u is given by $u = KSx_r$). This was important to avoid saturating the piezoactuator (the stack-piezo saturates if it is outside the $-10\ V$ to $0\ V$ range).

4.3 Characterization of the device

Figure 8 compares the bandwidth obtained by the PI, $\mathcal{H}_\infty$ designs and the ideal achievable bandwidth described earlier in the section. The $\mathcal{H}_\infty$ design improves the bandwidth by over sixty times when compared to the PI design. Also it provides a powerful paradigm for nanopositioning devices with a straightforward way of a prespecified tradeoff between bandwidth and resolution.

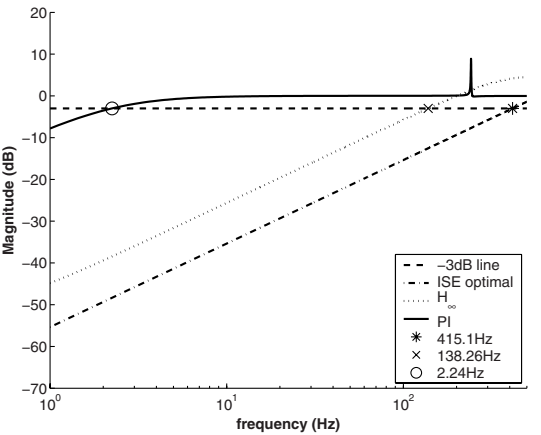

Fig. 8. Sensitivity functions obtained via the "ideal" controller, $\mathcal{H}_\infty$ controller and PI controller.

The device was calibrated by placing a calibration sample (which had 180 nm deep grooves every $5\mu m$) on the sample-holder and probing it by the AFM head. A triangular input of amplitude 2 V was given and the resulting LVDT output

showed the presence of 7.26 grooves. This implies the device has a static sensitivity of 18.15 $\mu m/V$. It was seen that the input voltage of approximately 4 V can be given without reaching the limits of the actuator. This guarantees a travel range of $70\mu m$.

As described earlier the accuracy of positioning using piezoactuators is greatly reduced due to nonlinear effects of hysteresis and creep. However, with $\mathcal{H}_\infty$ design, these effects are compensated and the closed loop device shows minimal hysteretic and creep effects.

Figure 9 compares the hysteresis curves for open and closed loop devices. The hysteresis effects which are predominant in large scans are as much as 10% (for full range) in the open loop device while they are nearly eliminated in the closed loop configuration. This also emphasizes the robustness of the closed loop design. Even though the controllers were designed for a nominal linear model obtained about a point (null position) in the operating range, the closed loop system works remarkably well even for scans that span the whole travel range of the device.

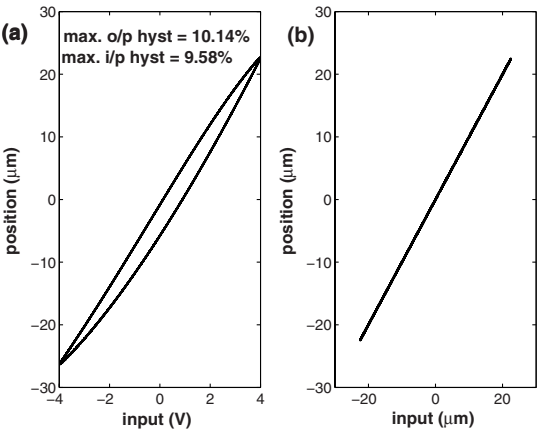

Fig. 9. Hysteresis in (a) the open loop configuration, (b) its elimination in the closed loop configuration.

Creep is another undesirable effect that becomes prominent in long time experiments. It is related to the effect of the applied voltage on the remnant polarization of the piezo ceramics. The piezoactuator starts drifting even at no application of any input signal to it. To measure this effect, we studied a step response of the device in open and closed loop configurations. We see that the output in the open loop case responds to the reference signal (see Figure 10(a)) but instead of reaching a steady state value it continues to decrease at a very slow rate. The response $y(t)$ was found to approximately satisfy the creep law with a creep factor of 0.55 The same experiment conducted in the closed loop (see Figure 10(a and b)) shows that the feedback laws virtually eliminate this effect and the system tracks the reference signal nearly exactly.

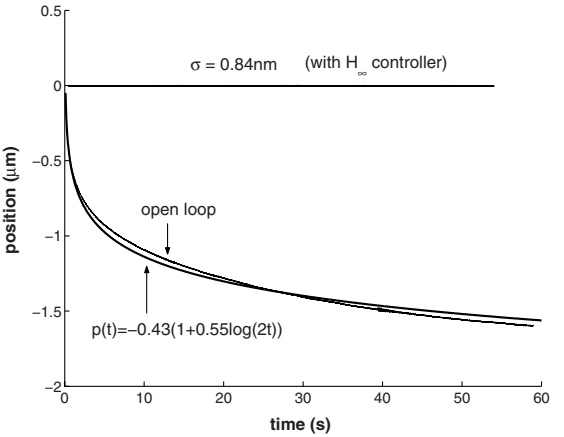

Fig. 10. The elimination of creep in the closed loop system and its approximation by a creep law.

These effects manifest themselves in lack of repeatability of the device. This is presented in Figure 11. Plot (b) shows the forward and backward scans put back to back of a calibration sample (shown in plot(a)) by using the device in the open loop configuration. This sample has equispaced grooves at every 5 μm. However, in the scans that we obtain, we see several inconsistencies: neither the grooves are equispaced, nor are they of same widths and also the forward and backward scans are not aligned. These mismatches can lead to gross errors and can be very misleading if these images are averaged to remove the effects of noise on the sample surfaces. In contrast, in the closed loop scan (see plot (c)), there is no mismatch and the forward and backward scan images match very well with the calibration sample.

5 Conclusions

Clearer understanding of tip-sample interactions and high speed, high precision sample positioning are essential for the interrogation and manipulation of materials using micro-cantilever based devices. A systems perspective is found to be very useful in addressing these challenges.

The AFM dynamics is presented as an interconnection of a linear system with a nonlinear feedback. The analysis of tapping-mode AFM dynamics reduces to the study of such a system being forced sinusoidally. This approach helps obtain tractable models for the tip-sample interaction and predicts the inherent limitations in the interrogation of sample using tapping-mode AFM. It is hoped that the systems perspective can be further exploited to develop observer based faster imaging schemes.

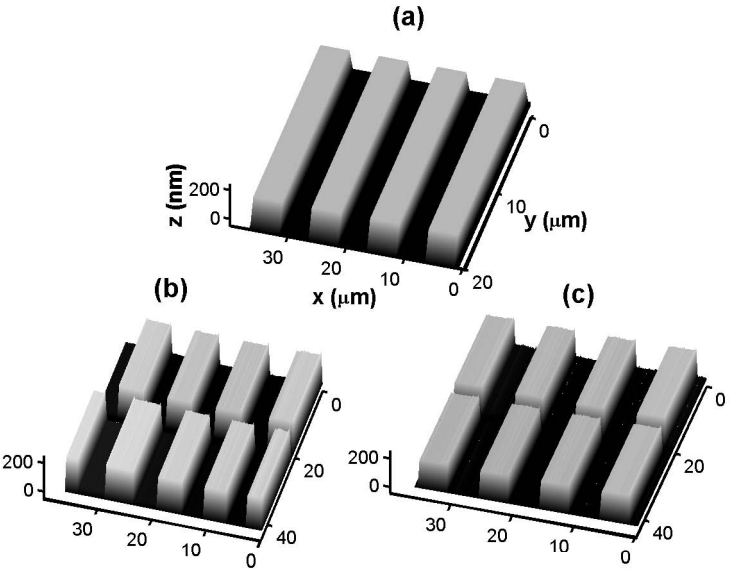

Fig. 11. (a) The reference (calibration sample) geometry. The grooves are separated by 5 μm and has a depth of 180 nm. (b) The mismatch in the position of grooves between the forward and the backward traverses in the open loop. (c) a good match in the closed loop configuration.

Broadband nanopositioning problem is shown to fit into the framework of modern robust control. In section 4, the design, identification and control of a positioning device is described.

Acknowledgements

This work is dedicated to Prof. Mohammed Dahleh. We would like to acknowledge the NSF grants: CAREER ECS-9733802 and CMS-0201560.

References

1. B. Anczykowski, D. Kruger, K. L. Babcock, and H. Fuchs. Basic properties of dynamic force spectroscopy with scanning force microscope in experiment and simulation. *Ultramicroscopy*, 66:251, 1996.
2. M. Ashhab, M. V. Salapaka, M. Dahleh, and I. Mezic. Dynamical analysis and control of micro-cantilevers. *Automatica*, 1999.
3. M. Ashhab, M. V. Salapaka, M. Dahleh, and I. Mezic. Melnikov-based dynamical analysis of microcantilevers in scanning probe microscopy. *Nonlinear Dynamics*, November 1999.

4. M. Benoit, D. Gabriel, G. Gerisch, and H. E. Gaub. Discrete interactions in cell adhesion measured by single-molecule force spectroscopy. *Nature Cell Biology*, 2(6):pp. 313–317, 2000.
5. N. A. Burnham, A. J. Kulik, G. Gremaud, and G. A. D. Briggs. Nanosubharmonics: the dynamics of small nonlinear contacts. *Physics Review Letters*, 74:5092–5059, 1995.
6. N. A. et. al. Burnham. How does a tip tap? *Nanotechnology*, 8:pp. 67–75, 1997.
7. U. Dammer, M. Hegner, D. Anselmetti, P. Wagner, M. Dreier, W. Huber, and H. J. Gntherodt. Specific antigen/antibody interactions measured by force microscopy. *Biophysical Journal*, 70:pp. 2437–2441, 1996.
8. U. Durig. Conservative and dissipative interactions in dynamic force microscopy. *Surface and Interface Analysis*, 27:pp. 467–473., 1999.
9. J. Fritz, M. K. Baller, H. P. Lang, H. Rothuizen, P. Vettiger, E. Meyer, H. J. Gntherodt, Ch. Gerber, and J. K. Gimzewski. Translating biomolecular recognition into nanomechanics. *Science*, 288:pp. 316–318, 2001.
10. A. Megretski and A. Rantzer. System analysis via integral quadratic constraints. *IEEE Transactions on Automatic Control*, 47, no.6:pp. 819–830., 1997.
11. A. Megretski and A. Rantzer. Harmonic analysis of nonlinear and uncertain systems. In *Proceedings of the American Control Conference*, Philadelphia, June 1998. Pensylvania.
12. M. Morari and E. Zafiriou. *Robust Process Control*. Prentice-Hall, Englewood Cliffs, 1989.
13. D. Rugar, C. S. Yannoni, and J. A. Sidles. Mechanical detection of magnetic resonance. *Nature*, 360:563–566, (1992).
14. M. V. Salapaka, H. S. Bergh, J. Lai, A. Majumdar, and E. McFarland. Multimode noise analysis of cantilevers for scanning probe microscopy. *Journal of Applied Physics*, 81(6):2480–2487, 1997.
15. M. V. Salapaka, D. Chen, and J. P. Cleveland. Linearity of amplitude and phase in tapping-mode atomic force microscopy. *Physical Review B.*, 61, no. 2:pp. 1106–1115, Jan 2000.
16. S. Salapaka, M. Dahleh, and I. Mezic. On the dynamics of a harmonic oscillator undergoing impacts with a vibrating platform. *Nonlinear Dynamics*, 24:pp. 333–358, 2001.
17. S. Salapaka, A. Sebastian, J. P. Cleveland, and M. V. Salapaka. High bandwidth nano-positioner: A robust control approach. *Review of Scientific Instruments*, accepted 2002.
18. A. Sebastian and M. V. Salapaka. Analysis of periodic solutions in tapping-mode afm: An IQC approach. In *International sysmposium on Mathematical Theory of Networks and Systems*, Notre Dame, IN, August 2002.
19. A. Sebastian, M. V. Salapaka, D. J. Chen, and J. P. Cleveland. Harmonic and power balance tools for tapping-mode atomic force microscope. *Journal of Applied Physics*, 89, no.11:6473–6480, 2001.
20. J. A. Sidles. Noninductive detection of single proton-magnetic resonance. *Appl. Phys. Lett.*, 58(24):2854–2856, 1991.
21. J. A. Sidles. Folded stern-gerlach experiment as a means for detecting nuclear magnetic resonance of individual nuclei. *Phys. Rev. Lett.*, 68:1124–1127, 1992.
22. J. A. Sidles, J. L. Garbini, and G. P. Drobny. The theory of oscillator-coupled magnetic resonance with potential applications to molecular imaging. *Rev. Sci. Instrum.*, 63:3881–3899, 1992.

23. S. Skogestad and I. Postlethwaite. *Multivariable Feedback Control, Analysis and Design*. John Wiley and Sons, 1997.
24. R. Wiesendanger. *Scanning Probe Microscopy and Spectroscopy*. Cambridge University Press, 1998.
25. V. A. Yakubovic. The matrix-inequality method in the theory of the stability of nonlinear control systems. *Avtomatika i Telemekhanika*, vol.25, no.7:1017–1029, 1964.